AIAA JOURNAL
Vol. 45, No. 3, March 2007

Experimental Investigation of Unsteady Thrust Augmentation Using a Speaker-Driven Jet

Daniel E. Paxson* and Mark P. Wernet*
NASA John H. Glenn Research Center, Cleveland, Ohio 44135
and
Wentworth T. John†
Ohio Aerospace Institute, Cleveland, Ohio 44135

DOI: 10.2514/1.18449

An experimental investigation is described in which a simple speaker-driven jet was used as a pulsed thrust source (driver) for an ejector configuration. The objectives of the investigation were twofold. The first was to expand the experimental body of evidence showing that an unsteady thrust source, combined with a properly sized ejector generally yields higher thrust augmentation values than a similarly sized, steady driver of equivalent thrust. The second objective was to identify characteristics of the unsteady driver that may be useful for sizing ejectors, and for predicting the thrust augmentation levels that may be achieved. The speaker-driven jet provided a convenient source for the investigation because it is entirely unsteady (i.e., it has no mean velocity component) and because relevant parameters such as frequency, time-averaged thrust, and diameter are easily variable. The experimental setup will be described, as will the two main measurements techniques employed. These are thrust and digital particle imaging velocimetry of the driver. It will be shown that thrust augmentation values as high as 1.8 were obtained, that the diameter of the best ejector scaled with the dimensions of the emitted vortex, and that the so-called formation time serves as a useful dimensionless parameter by which to characterize the jet and predict performance.

Nomenclature

A	=	jet area
d_{eff}	=	effective jet diameter
d_j	=	jet diameter
f	=	frequency
g_c	=	Newton constant
m	=	mass flow rate
P_{coil}	=	speaker coil power
p_{amb}	=	ambient pressure
p_e	=	exit pressure
Re	=	Reynolds number
T^j	=	thrust of the jet alone
T^{total}	=	total thrust of the combined jet and ejector
u	=	axial velocity component
u'	=	periodic fluctuating axial velocity component
V_{rms}	=	root-mean-square applied voltage
α	=	speaker chamber pressure coefficient
β_{ss}	=	steady mass entrainment ratio
β_{us}	=	unsteady mass entrainment ratio
η_{us}	=	unsteady augmentation efficiency
κ	=	speaker friction coefficient
μ	=	viscosity
ρ	=	density
σ	=	rms voltage to power conversion coefficient
τ_{cycle}	=	cycle time
τ_f	=	formation time
τ_f^{crit}	=	critical formation time
ϕ	=	thrust augmentation
ϕ_{ss}	=	steady thrust augmentation component
ϕ_{us}	=	unsteady thrust augmentation component

I. Introduction

UNSTEADY ejectors have received renewed attention in recent years, primarily due to the heightened interest in pulse detonation-based propulsion systems, which produce unsteady, impulsive thrust. It has been demonstrated in the past [1,2] and recently [3–8] that properly dimensioned ejectors, driven by unsteady thrust sources, often produce higher levels of thrust augmentation, at a considerably smaller size than do those driven by steady jets. For reference, thrust augmentation is defined as follows:

$$\phi \equiv \frac{\bar{T}^{\text{total}}}{\bar{T}^j} \tag{1}$$

The impetus for the experiment described in this paper was the observation that the recent demonstrations (experiments) referenced were inconsistent in their peak performance. A variety of thrust sources were used in [3–8], however, all shared a similar ejector style (nearly cylindrical). Parameters of the ejectors such as length, diameter, and inlet leading-edge radius were varied in each experiment in an effort to obtain sensitivities and to achieve a peak thrust augmentation configuration, which will be referred to in this paper as geometrical optimization. It was observed, however, that marked differences in peak augmentation levels were obtained with the different experiments. Even the same source operating at different frequencies yielded different augmentation levels.‡ This is shown in Fig. 1, where the peak thrust augmentation values obtained with the various thrust sources are plotted, along with their respective operational frequencies. The obvious conclusion to be drawn from this figure is that the presence of unsteadiness alone does not guarantee superior performance. There are characteristics of the unsteady jet which produce better or worse performance. Subsequent

Presented as Paper 0092 at the 42nd AIAA Aerospace Sciences Meeting, Reno, Nevada, 5–8 January 2004; received 30 June 2005; accepted for publication 5 October 2006.

*Aerospace Engineer, Instrumentation and Controls Division, MS 77-1. AIAA Associate Fellow.
†Senior Research Assistant, Instrumentation and Controls Division.

‡The pulse detonation engine (PDE) experiment [6] was not geometrically optimized as were those of [3–5,7,8]. Instead, a single ejector was used with a diameter-to-jet diameter ratio similar to both the optimized [3–5] experiments. This is consistent with the optimal findings of [9,10], where a similar sized PDE was used as a driver. The length used was the longest available at the time of the experiment. The inlet radius was also the largest available, a choice which is consistent with the experiment in [3].

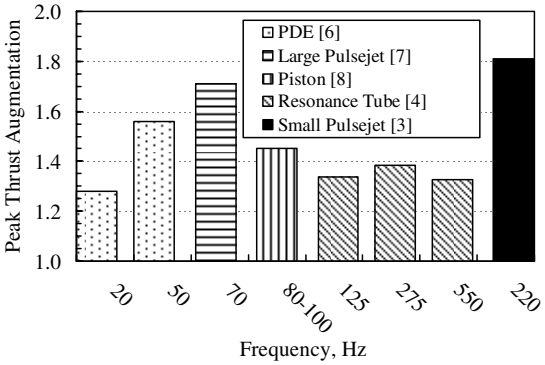

Fig. 1 Peak thrust augmentation levels achieved with various drivers using geometrically optimized, nearly cylindrical ejectors.

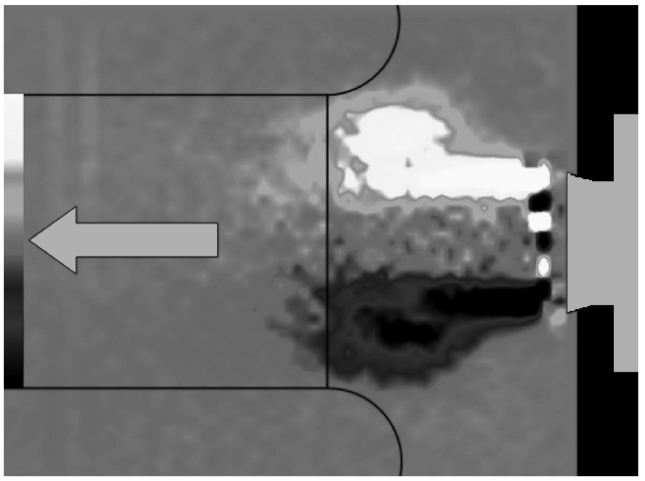

Fig. 2 Contours of 150 sample, phase-locked, ensemble-averaged, instantaneous vorticity in a pulsejet-driven flow.

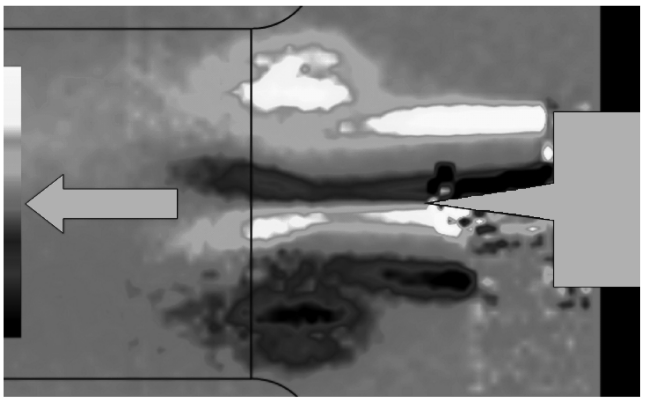

Fig. 3 Contours of 200 sample, phase-locked, ensemble-averged, instantaneous vorticity in a resonance tube-driven flow.

digital particle imaging velocimetry (DPIV) of both the pulsejet [3,11] and resonance tube [4] suggested that one critical feature of the flow is the vortex which is emitted with each pulse of the driver. Such vortices can be seen in Figs. 2 and 3 for each of the drivers [3,4], respectively. The figures show ensemble-averaged, instantaneous vorticity contours at the approximate moment when the emitted vortex would enter an ejector. Although not present when the PIV measurements were made, outlines of the ejector diameters yielding peak thrust augmentation are shown in each figure. In each case the optimal ejector is precisely sized to just bound the emitted vortex. This striking observation served to substantiate the notion that the starting vortex plays a vital role in the performance of unsteady ejectors, and furthermore, that parameters which characterize the vortex may characterize the ejector performance as well. One such parameter is the so-called formation time [12]. Its proposed use in predicting geometrically optimized ejector performance is briefly reviewed next from [3].

The thrust from an unsteady driver can be divided into a steady and an unsteady (but periodic) component. The thrust augmentation can similarly be divided. From this division, the total thrust augmentation can be expressed as

$$\phi = \frac{\phi_{ss} + (\overline{u'^2}/\overline{u^2})\phi_{us}}{1 + (\overline{u'^2}/\overline{u^2})} \tag{2}$$

where the jet velocity $u \equiv \bar{u} + u'$ (the contribution due to turbulence is assumed small in comparison to u', and is neglected) and where, if T is the thrust, then $\phi_{ss} = \overline{T}^{\text{total}}_{ss}/\overline{T}^{j}_{ss}$ and $\phi_{us} = \overline{T}^{\text{total}}_{us}/\overline{T}^{j}_{us}$. Here, overbars represent time averages. The steady-state augmentation component can be estimated using available correlations or mixing calculations. The unsteady thrust augmentation component, it is proposed, can be written in the form

$$\phi_{us} = (1 + \beta_{us})^{\eta_{us}/2} \tag{3}$$

This is a similar form to a model used for steady ejectors [13]. Both of the parameters in (3), and therefore the unsteady thrust augmentation itself, are thought to be sole functions of the jet formation time [12]. In this work, the formation time (an inverse Strouhal number or reduced frequency) is defined as

$$\tau_f = \frac{\sqrt{\overline{u'^2}}}{2 f d_j} \tag{4}$$

Equation (4) is a slightly different form than [12] from which it was obtained. In [12], the velocity and time scales were presented as

$$\int_0^{t_{\text{outflow}}} \text{u dt}$$

where t_{outflow} denotes the time period over which the flow is leaving the jet source. This is often a difficult quantity to obtain, and may not be appropriate when the unsteady jet source has a large steady component of velocity. In jets where the steady velocity component is small, it is probable that the preceding integral is closely related to $\sqrt{\overline{u'^2}}/2d_j f$. It is noted that $\overline{u'^2}$ is impossible to measure directly in some experiments, but can be inferred from thrust data, or estimated from simulations. With β_{us} a monotonically increasing function of τ_f and η_{us} flat to some critical value of τ_f^{crit}, then monotonically decreasing (based on limited data from [3,4]), the form of ϕ_{us} becomes that shown in Fig. 4. Also shown in this figure are the available results measured from several experiments. The smooth curve represents heuristic modeling of β_{us} and η_{us}, fit to available data, and used in Eq. (3) [3]. The comparison between predictions and experiment is encouraging, particularly with regard to the basic shape. There appears to be a particular formation time at which the

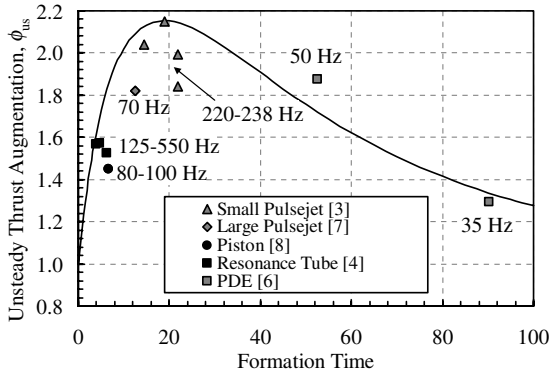

Fig. 4 Unsteady thrust augmentation for optimized ejector/driver configurations using a variety of drivers.

best unsteady performance is found, with performance falling off rapidly to the left and gradually to the right. The data, however, are admittedly sparse. The sparse nature of the data was, in fact, the impetus for the experiment to be described.

If an unsteady thrust source could be developed with the capability of large variations in frequency, $\overline{u'^2}$, and jet diameter, then a range of formation times could be examined. This could be used to validate the notion of formation time as a performance correlating parameter because it could be varied in several ways (e.g., diameter, frequency, and $\overline{u'^2}$).

A speaker-driven, or so-called synthetic, jet meets these requirements and has the added benefit of having no steady velocity component (zero net mass flow), thereby isolating the thrust augmentation to only the unsteady component.

One potential drawback to the device is that the thrust levels and corresponding velocities are exceptionally low, possibly putting the flow in a different regime from the other devices examined. This will be discussed in subsequent sections.

This paper describes the speaker-driven jet experiment and presents the results obtained to date. It will be shown that formation time as previously defined is an excellent correlating parameter (i.e., much of the data collapse onto a single curve when plotted as a function of τ_f). It will also be shown, however, that it is not the only required parameter. There are apparently additional characteristics of the jet flow that impact performance because the peak thrust augmentation levels achieved with the speaker-driven jet were below those seen in Fig. 1. Possible explanations will be offered.

Additionally, limited results from particle imaging velocimetry (PIV) measurements obtained on the system will be presented to supplement discussions and assumptions. No description of the PIV system or method will be presented as it is well described elsewhere [11].

II. Experimental Setup

The experimental arrangement is shown to scale in Fig. 5, along with relevant nomenclature. An 8 in., dual coil speaker (Peerless brand) was mounted on the back of a cylindrical cavity. The other end of the cavity was sealed except for an exit orifice, the diameter of which could be varied by means of the inserts shown. The speaker was driven by an Altec/Lansing Model 1269 audio amplifier. The input signal for the amplifier was a sinusoid of variable frequency supplied by a Wavetek Model 193 signal generator. The speaker and cavity arrangement was mounted on a support stand from which an ejector could be suspended. Below this, an 18 in. square plexiglass plate was mounted on a Mettler-Toledo Model PB5001-S digital scale (with 0.1 g accuracy). The scale rested on the floor of the laboratory. All measurements of thrust were made by simply reading the output on the scale. This was the only method available, and was suboptimal due to the fact that readings were often fluctuating. A long-duration, time-averaging procedure would have been preferable, however, given the large number of readings obtained, it is believed that the overall error introduced by the method used is small. Output from the audio amplifier was measured on a Tektronix Model TDS-220 oscilloscope, from which both frequency and root-mean-square (rms) voltage could be obtained.

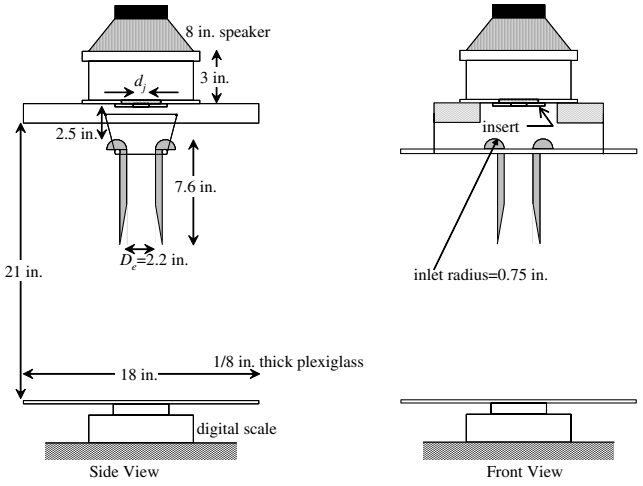

Fig. 5 Experimental setup and nomenclature for the speaker-driven jet.

III. Jet Characterization

The system was initially tested with no ejector in place so that the denominator of Eq. (1) could be determined. Typical results are shown in Fig. 6 where measured thrust is plotted against rms voltage for various jet diameters, at a driving frequency of 20 Hz. Dynamic analysis of the system is straightforward with the exception of the speaker voice coil. If the coil is replaced by a sinusoidal forcing function, and the flow from the orifice is assumed to obey an incompressible Bernoulli-type relation, the analysis indicates that over the frequency range tested, the velocity of the speaker cone is in phase with the flow velocity at the orifice (i.e., at the exit). Therefore, because the thrust produced by the system is proportional to the mean square of exit flow velocity, it may be shown that the average power from the coil must be

$$\bar{P}_{\text{coil}} = \frac{\alpha}{d_j}(\bar{T}^j)^{1.5} + \kappa d_j^2 \bar{T}^j \tag{5}$$

The first term on the right describes the power consumed in developing pressure in the system chamber. The second term describes the power consumed by mechanical friction. Although the impedance characteristics of the voice coil are complex, it is reasonable to expect that, for a given frequency, the average mechanical power supplied is proportional to the square of the applied rms voltage. Thus, Eq. (5) may be modified as follows

$$V_{\text{rms}} = \sigma\sqrt{\bar{T}^j}\left(\frac{\alpha}{d_j}\sqrt{\bar{T}^j} + \kappa d_j^2\right)^{1/2} \tag{6}$$

This equation is shown in Fig. 6 for $d_j = 1.2$ in. Initial values for σ, α, and κ were measured on the system, then adjusted to fit the data. It is clear that the form of Eq. (6) fits the data well and adds a measure of confidence to the measurements. However, the desired relationship for further study is jet thrust as a function of applied voltage. By plotting Eq. (6) with jet thrust as the dependent variable, it was found that a nearly perfect fit was obtained using a cubic polynomial of the form

$$\bar{T}^j = a_1 V_{\text{rms}} + a_2 V_{\text{rms}}^2 + a_3 V_{\text{rms}}^3 \tag{7}$$

Data from each configuration (i.e., d_j and f) of the data sets were therefore fit with such a polynomial, and these are shown in Fig. 6. For the more than 300 data points collected, the standard deviation

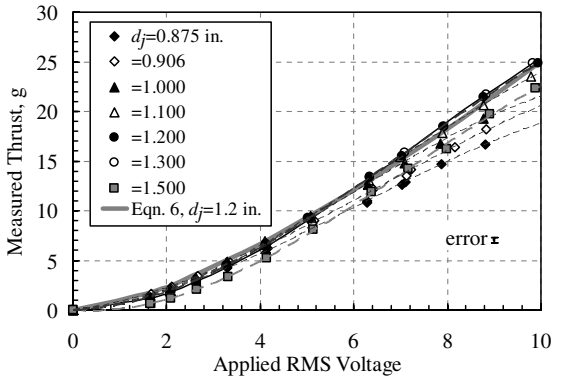

Fig. 6 Measured, time-averaged jet thrust as function of RMS speaker voltage.

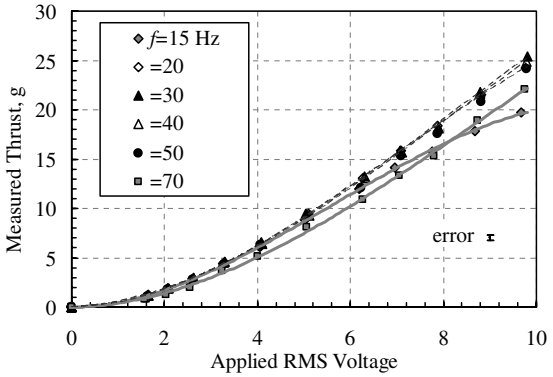

Fig. 7 Measured, time-averaged jet thrust as function of RMS speaker voltage.

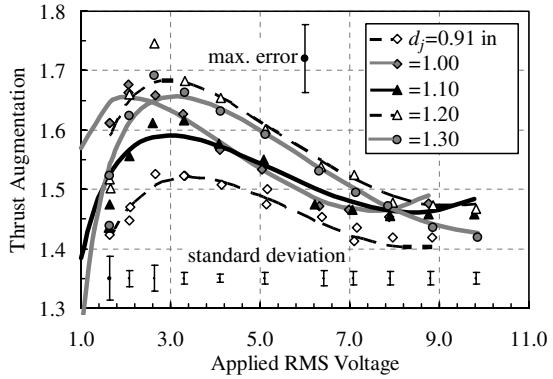

Fig. 8 Measured, time-averaged thrust augmentation as function of RMS speaker voltage for various jet diameters.

between measurement and prediction was found to be 0.137 g. Approximately 95% of all the data collected fell within two standard deviations. Thus, the thrust measurement error is 0.275 g.

It is observed that for a given rms voltage excitation, the thrust increases with increasing jet diameter until $d_j = 1.5$ in., where it decreases. This trend is predicted by Eq. (5) and represents a shifting of power consumption from generating thrust to mechanical damping in the speaker. It is noted that Eq. (5) predicts a finite thrust as the exit diameter approaches that of the speaker. However, it was observed that beyond $d_j \cong 5$ in., no thrust was observed in the range of rms voltages tested. One reason for this may be as follows. Although a pulsed system such as the one described here is a so-called zero net flow device, it cannot generate thrust unless the mass of fluid expelled during one portion of the cycle is distinct from that which is taken in during the remainder of the cycle. Stated another way, if fluid exits the device, reverses, and is reingested in within one cycle, it does not contribute to thrust. For most operating conditions of the system, such flows do not occur. The majority of the expelled gas is carried downstream by the emitted vortex ring and by the momentum of the trailing jet. Ingestion is largely potential, coming from all directions. However, in cases where the orifice diameter is large, or the speaker cone displacement is exceedingly small (i.e., $\tau_f \ll 1$), reingestion may occur resulting in lost or nonexistent thrust.

If this explanation is valid, it could be a contributing factor to the lost thrust observed with $d_j = 1.5$ in. Such an exhaust flowfield would change the nature of the subsequent interactions with the downstream ejector, thereby producing anomalous results. Because of this possibility, thrust augmentation data were collected only for jet diameters smaller than this.

Figure 7 shows measured thrust plotted against rms voltage for various frequencies, at a jet diameter of 1.2 in. Here, it is seen that thrust obtained for a given excitation is essentially independent of frequency from $20 < f < 50$ but falls off substantially above or below this range. At low frequency, the thrust reduction appears to be related to the speaker coil reaching fixed travel limits. The reason for the high frequency reduction is not entirely clear. It is probable that changes in the coil impedance are contributing. It is not predicted by the dynamic analysis described previously with the coil removed. It is noted that at approximately 200 Hz there is no measurable thrust. This is consistent with the reingestion phenomenon described earlier. Whatever the mechanism behind the changes in thrust for a given excitation, the frequencies at which they occurred were deemed as limits for augmentation testing. Thus, augmentation results (i.e., thrust with an ejector) were collected at frequencies between 15 and 70 Hz.

IV. Augmentation

Only one ejector diameter was tested in this experiment. Because of the peculiarities of the setup, it was much easier to obtain geometric optimization by varying the driver jet diameter than by varying the ejector diameter as was done in [3,4]. The ejector inlet radius (see Fig. 5) was set at 0.75 in. and no testing was done to determine an optimal value. Previous experiments indicate that, in general, the bigger the radius, the better the performance; however, beyond a configuration dependent value, the dependence is very weak. Because it was difficult to change the position of the ejector, all augmentation measurements were made at a driver-to-ejector inlet spacing of approximately 2.5 in. This effect is also expected to be fairly small based on previous results.

For each jet diameter and frequency, thrust as a function of rms voltage was first determined for the jet alone and fit to a cubic least squares approximation as described earlier. The ejector was then put in place and thrust (now total) was again measured against excitation voltage. From these data, and the cubic fit, thrust augmentation was determined.

The symbols in Fig. 8 show thrust augmentation calculated in this fashion as a function of the rms excitation voltage for several jet diameters. The ejector length is 7.6 in. The data were obtained at an excitation frequency of 20 Hz. In general, a jet diameter of 1.2–1.3 in. yielded the highest augmentation over the range of excitation voltage. Similar results were found at frequencies of 30 and 40 Hz. The next largest jet diameter insert available was 1.5 in. which, as noted in Fig. 6, produced somewhat anomalous results and was not used for augmentation studies. Thus, the 1.2 in. jet was chosen as being geometrically optimized for the ejector and was used in subsequent tests to vary formation time. This jet diameter was also used in tests to determine the optimal length of the ejector. Three different length ejectors were tested over a limited set of frequencies. Of these, the 7.6 in. length ejector shown in Fig. 5 yielded the best results.

The total thrust of the ejector and jet was also fit to a fourth order polynomial for each jet diameter tested. This choice of fit resulted in the lowest error between measurement and prediction. As with the jet alone, 95% of all the data collected fell within two standard deviations. The total thrust measurement error is therefore estimated as 0.275 g. The polynomial fit to the total thrust was then divided by the fit to the jet alone to produce estimated thrust augmentation curves. These curves are shown as the smooth lines of Fig. 8. The standard deviation between these estimates and the measured values for all ejectors tested was 0.029. All of the deviations fell within two standard deviations. Figure 8 also shows the standard deviation of predicted and measured thrust augmentation at each excitation voltage. The values are significantly larger at lower excitation levels. This is an expected trend. Because thrust levels decrease with lower excitation voltage, and thrust augmention is a ratio of thrusts, small measurement errors on the order of 0.2 g have a large effect on calculated thrust augmentation.

Subsequent PIV measurements on this jet yielded results similar to those noted in Figs. 2 and 3, namely that the boundary of the emitted vortex coincides with the optimally performing ejector diameter. This is illustrated in Fig. 9 which shows 200 point ensemble-averaged, instantaneous contours of vorticity for the emitted vortex of the 1.2 in. jet at a frequency of 50 Hz and an rms speaker excitation voltage of 10.0 V. An outline of the ejector is also shown, but was not present during velocity measurements. Identical images were obtained at 20 Hz excitation.

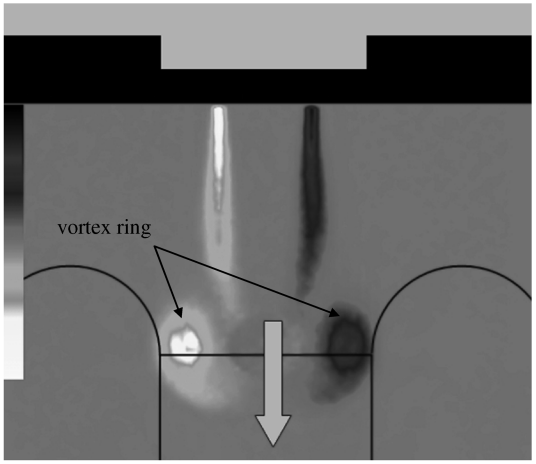

Fig. 9 Contours of 200 sample, ensemble-averaged, instantaneous vorticity in a speaker-driven flow.

It is observed that ratio of ejector body diameter (2.2 in.) to driver diameter (1.2 in.) yielding optimal performance is quite different, at 1.83, than those of other unsteady driver experiments, which range from 2.4–3.0. This observation suggests that a speaker-driven vortex may scale in size somewhat differently than one emanating from a "pipe" such as a pulsejet, resonance tube, or pulse detonation engine. This will be discussed in the next section of the paper.

V. Calculation of Formation Time

The formation time defined by Eq. (4) requires an rms velocity, which generally must be inferred or computed based on available data. A momentum balance will show that for a speaker-driven jet with no net mass flow, the approximate time-averaged thrust is

$$\bar{T}^j = \left(\frac{\rho A}{g_c}\right)\overline{u'^2} + \frac{A}{\tau_{\text{cycle}}}\int_0^{\tau_{\text{cycle}}} (p_e - p_{\text{amb}})\,\mathrm{d}\tau \tag{8}$$

During outflow periods, it may be reasonably assumed that $p_e = p_{\text{amb}}$ [14]. During inflow periods, it is estimated that $p_e - p_{\text{amb}} \approx -\rho\overline{u'^2}/2g_c$. Thus, with inflow occurring over approximately half the cycle

$$\bar{T}^j \cong 0.75\left(\frac{\rho\pi d_j^2}{4g_c}\right)\overline{u'^2} \tag{9}$$

Equations (8) and (9) assume a spatially uniform distribution of pressure and rms velocity across the jet, however, it was observed in the PIV measurements that this was not the case. This is clearly seen in Fig. 10 which shows the measured distributions of rms velocity for two different sized jets, at two different formation times. Each point is a time-average of 16 phase-locked instants comprising a full cycle. Each instant consists of 200 ensemble-averaged measurements. The measurements are 0.2 in. downstream of the jet exit. The physical boundaries of the jet openings are shown with solid vertical lines. All of the rms distributions appear to have a nearly uniform region that is smaller than the physical jet diameter. Because it is this "core" flow that is of importance in vortex formation, it seems reasonable to characterize the jet not by the physical diameter or area, but by an effective diameter, and to use the core rms velocity fluctuations to determine formation time. For both of the jets measured it was found that

$$d_{\text{eff}} = d_j\sqrt{0.6} \tag{10}$$

Interestingly, this corresponds closely to a typical discharge coefficient for a sharp-edged orifice in steady flow. It is also interesting to note that using this effective diameter makes the ratio of ejector to (effective) jet diameter at which peak performance occurs 2.4, which is nearly identical to that found with the pulsejet-driven system. That is to say, it reinforces the growing evidence that optimal unsteady ejectors scale in diameter with the vortex, and that the vortex scales in size with the effective jet source.

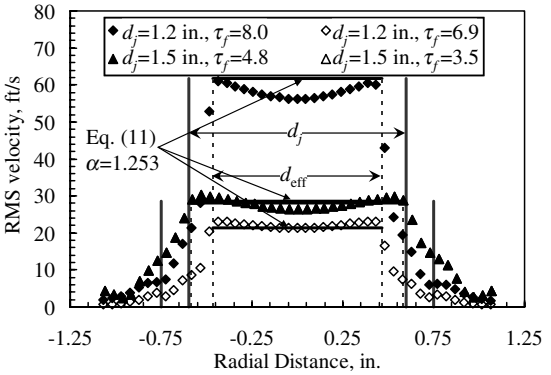

Fig. 10 RMS velocity as a function of radial distance for several jets.

In light of the observed nonuniformities in rms velocity, the observed presence of an effective diameter, and the fact that it is an estimate, Eq. (9) was modified, and rearranged to solve for rms velocity as

$$\sqrt{\overline{u'^2}} = \frac{1}{d_{\text{eff}}}\left(\frac{\bar{T}^j 4g_c}{\alpha\rho\pi}\right)^{1/2} \tag{11}$$

where it is understood that the rms velocity referred to is the jet core value. The coefficient α was determined for each of the four jet velocity fields measured using PIV and the corresponding measured thrust values. Averaging the four α values yielded a final result of $\alpha = 1.253$, with a standard deviation of 7%. The rms velocity values calculated with Eq. (11) and this α for the four jets measured with PIV are shown in Fig. 10.

VI. Results

Formation time, as described in the preceding section, and thrust augmentation, were obtained for the 1.2 in.-diam jet and 2.2 in.-diam ejector over a range of frequencies from 15 to 70 Hz, and over a range of jet thrust levels from 0 to 25 g. The data were used to make the plot shown in Fig. 11. Here, thrust augmentation (unsteady by definition) is plotted as a function of jet formation time for the entire frequency and thrust range tested. The fact that all of the data collapse neatly on a single curve is strong evidence that the formation time of Eq. (4) is indeed a relevant parameter for predicting geometrically optimized ejector performance. The curve shown in Fig. 11 is simply a polynomial fit to the data, however, it is remarkably similar in shape to that formed by Eq. (3) and its underlying assumptions (i.e., entrainment increases with τ_f, and efficiency is initially flat then decreasing with τ_f). This result lends a measure of credence to such a modeling approach.

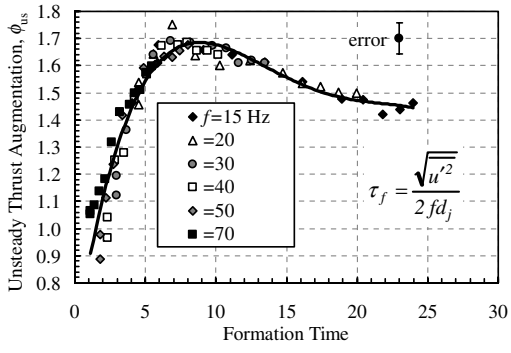

Fig. 11 Thrust augmentation as a function of the formation time.

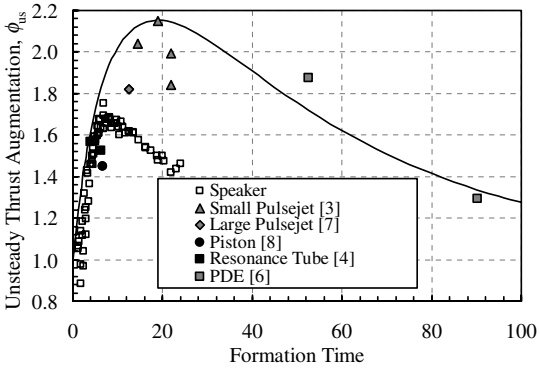

Fig. 12 Unsteady thrust augmentation as function of formation time for tested thrust sources.

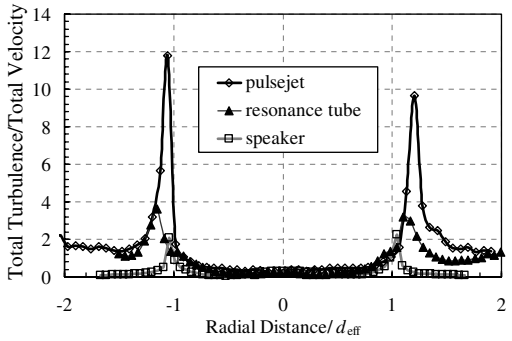

Fig. 13 Total turbulence distributions for three separate pulsed thrust sources.

VII. Discussion

Although Fig. 11 demonstrates a consistent relationship between the formation time and thrust augmentation for the speaker-driven jet, it is somewhat inconsistent with results obtained using other unsteady data. Figure 12 combines the results of Figs. 4 and 11 onto a single plot. Here it is seen that while the speaker-driven system has the same trend as the other systems, the peak values are not as high and the formation time at which the peak occurs seems to be somewhat lower. With regard to the latter discrepancy, it should be kept in mind that the values of $\sqrt{\overline{u'^2}}$ used in calculating the formation times of the other experiments are estimated from equations similar to Eq. (11). Whereas this proved accurate for the speaker-driven jet, it may not prove reliable for the other thrust sources. Subsequent PIV measurements on the resonance tube and pulsejet sources, for example, showed values of $\sqrt{\overline{u'^2}}/\bar{u}$ to be approximately 0.83 and 1.74, respectively. These were somewhat less than the estimated values of 1.04 and 1.89. This result reduces the formation time (but raises the unsteady thrust augmentation) for both cases. Furthermore, in the case of the pulsejet and PDE, the density [used in Eq. (11)] of the emitted flow could not be measured. Estimates based on simulations were used, and these may have inaccuracies too.

Regarding the differences in peak thrust augmentation values between the present and previous experimental results, several mechanisms seem plausible and will be discussed next.

A. Reynolds Number

The vorticity transport equations (being derived from the Navier–Stokes equations) yield a dissipation term that is preceded by a Reynolds number. For the unsteady jets under consideration here, an appropriate Reynolds number may be written

$$Re = \frac{\bar{\rho}\sqrt{\overline{u'^2}}\, d_{\text{eff}}}{\bar{\mu}} \tag{12}$$

The typical values for the four experiments are shown in Table 1, along with the peak unsteady thrust augmentation levels obtained. Although the pulsejet has rms velocities that are an order of magnitude above the speaker-driven system, the emitted flow is much hotter and therefore much less dense, and much more viscous. The result is that the two systems have comparable Reynolds numbers but much different performance. Conversely, the speaker-driven and resonance-tube systems have vastly different Reynolds numbers, but similar performance. It is therefore unlikely that this is the explanation for the differences; however, it is noted that the length and velocity scales used to define the Reynolds number shown may not be appropriate.

Table 1 Reynolds number estimates for several pulsed thrust experiments

	Speaker-driven	Pulsejet	Resonance tube	PDE
$Re \times 10^4$	3.0	3.5	25	18
ϕ_{us} (max.)	1.70	2.14	1.56	1.88

B. Turbulence

Here again, the impact is unclear; however, it is noted that the pulsejet, which showed the highest thrust augmentation, has a vortex which is considerably more turbulent than the others for which such measurements were possible. Figure 13 shows the instantaneous, ensemble-averaged, total turbulence distributions for three separate pulsed thrust sources. Turbulence has been scaled by local, instantaneous, ensemble-averaged, total velocity. Note that the turbulence shown is distinct from the periodic velocity fluctuation used in calculating formation time. Radial distance has been scaled by effective diameter. The measurements were made using PIV at the approximate downstream location where the vortex enters the ejector. Of note in the figure is the observation that the regions of high vorticity are the same as those of high turbulence and that the pulsejet-driven flow has particularly high values. It is possible that the turbulence in this region acts as an effective mechanism by which the vortex transfers its rotational energy to the entrained flow. Alternately, the turbulence may act to enhance entrainment of secondary flow by the vortex.

It is probable that the high turbulence level of the pulsejet flow result from the violent combustion processes taking place within the device. It is probable that these are present in the PDE as well, which is consistent with the relatively high augmentation results observed.

It is interesting to note that preliminary computational simulations of a PDE-driven ejector system similar to the one actually tested [6], but using an inviscid code, yielded no thrust augmentation.[§] The addition of laminar viscosity may make little difference to such a calculation, however, high levels of turbulent viscosity may have a substantial impact.

C. Emitted Flow Enthalpy

It is observed that the pulsed sources with the highest emitted specific enthalpy seem to yield the highest unsteady thrust augmentation. No explanation can yet be offered as to why this is so. In fact, steady ejector analysis indicates a reduction in performance as the enthalpy increases relative to the entrained flow. Even without explanation, however, it was deemed worthwhile to explore ways to test this observation with the present speaker-driven system.

One simple way is shown in Fig. 5. The system was modified such that a steady flow of a low molecular weight gas could be introduced into the cavity region. The modified setup is shown schematically in Fig. 14. The gas chosen was helium. The jet diameter was 1.2 in. Conceptually, ambient air enters the cavity on the "in-stroke" of the speaker, mixes with whatever helium is forced into the cavity, and exits on the "out-stroke" as a uniform mixture at some intermediate density and specific enthalpy. Because of time constraints, no provision was made to directly measure the degree of mixing or the precise enthalpy of the emitted gas. Nevertheless, the enthalpy could

[§]From personal communications with Shaye Yungster, Aug. 2003.

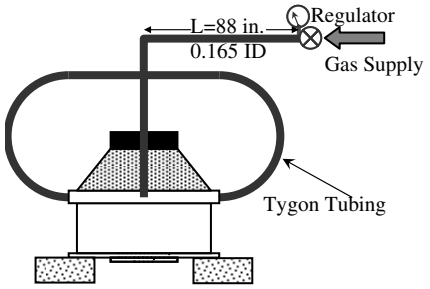

Fig. 14 Schematic diagram of modified speaker-driven jet allowing forced addition of supplementary gas.

be estimated, as will be shown, and a lack of uniformity in the exit flow will not substantially affect the establishment of a link between driver enthalpy and thrust augmentation.

Although no flow meter was available, a pressure regulator at the gas supply point, followed by 88 in. of 0.165 in. i.d. tubing, allowed for reasonable estimates using a Moody chart [15].

Because of the limited supply of helium in the facility, testing was limited to only one operational frequency. The value chosen was 15 Hz to obtain the highest possible formation times. Higher formation times were sought because Fig. 12 indicates that peak thrust augmentation occurs at higher formation times for higher enthalpy jets. At the 15 Hz frequency, two speaker excitation voltages were tested. These were rms voltages of 2.63 and 8.79 V.

The jet was first tested alone at various levels of auxiliary gas injection using both air and helium. The two gases were used to distinguish between changes in thrust due to using a light (high specific enthalpy) gas and those due to auxiliary injection itself. The results are shown in Fig. 15. Here, the measured jet thrust is plotted as a function of estimated auxiliary gas volumetric flow rate for both helium and air as auxiliary gases, using the two different excitation voltages. Each point is an average of several readings, with data scatter typically less than 0.3 g. The estimated auxiliary flow rate has been normalized by the product of the effective area and the rms velocity of the jet with no auxiliary gas present [Eq. (11)]. Values of this normalized flow rate that are greater than one roughly indicate that the auxiliary gas flow completely fills the added chamber volume during the intake stroke of the speaker. That is, there is no longer inflow through the jet opening. Also shown in the figure (as open symbols), for air only, are the expected thrust levels if the estimated steady flow components were simply added to the unsteady component when there is no injection.

Several features of this plot are surprising, and tend to render the augmentation results which follow somewhat inconclusive, though still worthwhile. Consider first the results with air as auxiliary gas. It was expected that the addition of auxiliary air would lead to an increase in thrust, because it adds a component to Eq. (9). Whereas this seems to hold well for the low-voltage excitation, it does not for the high-voltage case. The latter result suggests that the presence of the auxiliary air has an impact on the motion of the speaker itself and, in turn, on the manner in which fluid moves into and out of the cavity.

A second, and perhaps more striking, feature of Fig. 15 is the apparent negative thrust (lift on the thrust plate of Fig. 5) observed in the low-voltage case, with helium as the auxiliary gas. This is most likely related to buoyancy effects, which can influence the thrust measurements due to the particular orientation of the thrust plate and jet (i.e., it is pointing toward the ground). The negative thrust may arise when the lightweight gas jet forms a sheet as it is deflected across the thrust plate. Alternately, the gas may never become a sheet. It may begin to spread across the thrust plate, then rise from it. Both situations could give rise to a negative thrust reading. It should be kept in mind as well that at the low speaker excitation levels, the emitted flow is composed entirely of helium (see Fig. 15). Thus, based on density alone, the thrust should be approximately seven times less than that measured with air as the auxiliary gas. Extrapolating the air results of Fig. 15 to auxiliary flow rates comparable to those with helium would therefore yield a maximum thrust of only about 1 g. A small error due to buoyancy could easily lead to negative readings. Additionally, if the emitted flow from the jet is thought of as a series of self-contained "balls" of helium, the deceleration due to their buoyancy could result in them moving significantly slower by the time they reach the plate than when they left the exit hole of the jet. This, in turn would lead to a thrust reading even less than the 1.0 g estimate just given.

Because of the large error introduced by buoyancy effects, the low-voltage excitation data were not considered usable, and all of the results shown hence will focus on the high-voltage data. It is noted, with respect to the high-voltage excitation data, that the decrease in thrust observed with the helium auxiliary gas is consistent with the emitted gas being less dense. Buoyancy effects are expected to be lower in this case, however, as the emitted gas is not nearly as light as the low-voltage case. Furthermore, the thrust levels are much higher, and the errors, even if the same as the low-voltage case, are a considerably smaller fraction of the total.

Thrust augmentation results for the high-voltage case are presented in Fig. 16. Like Fig. 15, data is plotted as a function of estimated auxiliary gas volumetric flow rate. The trend of the auxiliary air data is expected in light of Eq. (2). As more gas is injected, the steady component of thrust rises. The thrust augmentation due to this steady component is considerably less than the unsteady component, and thus the overall augmentation should decrease. The trend for auxiliary helium data seems to support the notion that high enthalpy jet flows improve the unsteady thrust augmentation.

An estimate of the jet density and hence specific enthalpy may be obtained as follows. Assuming that thrust may be calculated as

$$\bar{T}^{\,j} \cong \left(\frac{\rho\pi d_{\text{eff}}^2}{4g_c}\right)(\overline{u'^2} + \bar{u}^2) \tag{13}$$

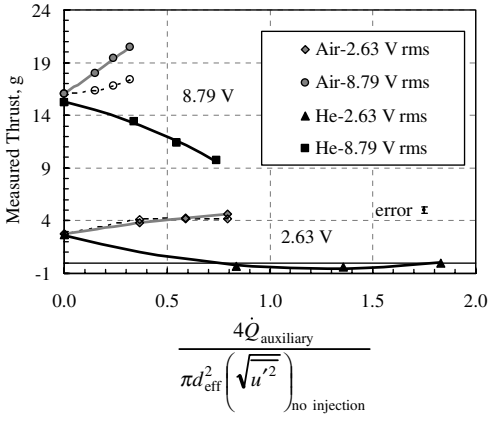

Fig. 15 Measured jet thrust as a function of estimated auxiliary gas flow rate.

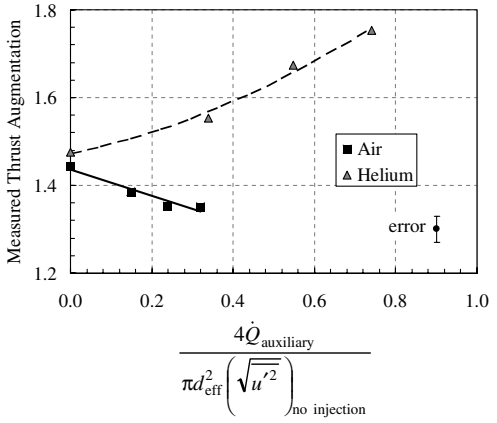

Fig. 16 Measured thrust augmentation for the modified speaker-driven jet at 8.79 V.

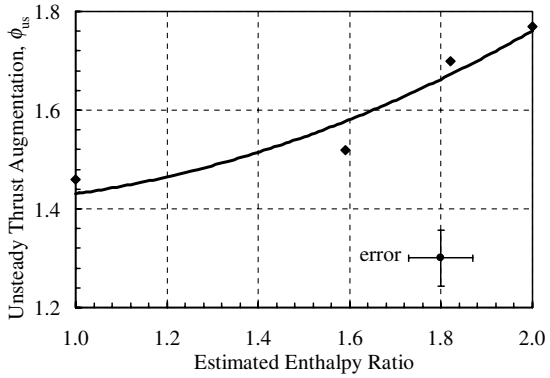

Fig. 17 Derived unsteady thrust augmentation for the modified speaker-driven jet at 8.79 V.

For the jet with auxiliary air injection, ρ, and $\bar{u}$ are known (the latter from the estimated auxiliary flow rate). Equation (13) can thus be used to obtain $\overline{u'^2}$. This value was a nearly constant 3652 ft^2/s^2 for the three air injection cases tested, with only 3.8% standard deviation. Assuming this same value of $\overline{u'^2}$ for the helium auxiliary gas and noting that

$$\dot{m}_{\mathrm{He}} \approx \frac{\bar{\rho}\,\bar{u}\,\pi d_{\mathrm{eff}}^2}{4} \tag{14}$$

Equations (13) and (14) (with $\rho = \bar{\rho}$) can be solved simultaneously to obtain $\bar{\rho}$ and $\bar{u}$. These can, in turn, be used to obtain the average specific enthalpy ratios (from the properties of helium and air mixtures) and the values of unsteady augmentation from Eq. (2). A steady thrust augmentation estimate (based on a simple constant area mixing calculation) of 1.2 is used. This exercise results in the plot shown in Fig. 17 where unsteady thrust augmentation is plotted as a function of jet enthalpy ratio. The data are limited and the potential error is large due to the assumptions and estimates described earlier, however, the trend is clear. For this experiment, and within the range shown, thrust augmentation does indeed increase with increasing enthalpy ratio.

VIII. Conclusions

The experiment described in this paper has demonstrated that a versatile, small scale, speaker-driven, pulsed-thrust system can be used to investigate unsteady thrust augmentation in general. It was verified that the formation time, as defined in Eq. (4), is a relevant, though not sufficient, parameter on which to base unsteady ejector performance. Furthermore, it was demonstrated that unsteady thrust augmentation, plotted as a function of formation time, exhibits a maximum value as predicted by the modeling approach of Eq. (3). The critical formation time, at which the maximum occurs, is close to that identified in [10] as marking the point when the emitted vortex no longer contains all of the emitted vorticity. Results indicate that the jet-to-ambient enthalpy ratio may be another critical parameter in predicting unsteady thrust augmentation.

The DPIV measurements presented strongly suggest that the ejector diameter for which optimal augmentation is obtained is directly linked to geometric size of the vortex ring, and that the vortex ring size is geometrically related to the (effective) jet diameter. In this work, it was found that the optimal ejector diameter is approximately 2.4 times that of the driver. It was also concluded from these measurements that vortex turbulence may play a role in unsteady ejector performance.

References

[1] Lockwood, R. M., "Interim Summary Report on Investigation of the Process of Energy Transfer from an Intermittent Jet to Secondary Fluid in an Ejector-Type Thrust Augmenter," Hiller Aircraft Rept. No. ARD-286, March 1961.

[2] Binder, G., and Didelle, H., "Improvement of Ejector Thrust Augmentation by Pulsating or Flapping Jets," Paper E3 of *Proceedings 2nd Symposium on Jet Pumps and Ejectors and Gas Lift Techniques*, Cambridge, England, March 1975.

[3] Paxson, D. E., Wilson, J., and Dougherty, K. T., "Unsteady Ejector Performance: An Experimental Investigation Using a Pulsejet Driver," AIAA Paper 2002-3915, July 2002.

[4] Wilson, J., and Paxson, D. E., "Unsteady Ejector Performance: An Experimental Investigation Using a Resonance Tube Driver," AIAA Paper 2002-3632, July 2002.

[5] Wilson, J., "A Simple Model of Pulsed Ejector Thrust Augmentation," NASA CR 2003-212541, Aug. 2003.

[6] Thomas, S., Deloof, R., and Dougherty, K., "Review of the NASA Glenn Research Center Pulse Detonation Engine Technology (PDET) Project," presented at *14th Annual Symposium on Propulsion, University Park, PA*, 10–11 Dec. 2002.

[7] Paxson, D. E., Litke, P. J., Schauer, F. P., Bradley, R. P., and Hoke, J. L., "Performance Assessment of a Large Scale Pulsejet-Driven Ejector System," AIAA Paper 2006-1021, Jan. 2006.

[8] Mason, S. A., and Miller, R. J., "Performance of Ejectors Driven by Sinusoidally Unsteady Jets,"AIAA Paper 2006-1020, Jan. 2006.

[9] Rasheed, A., Tangirala, V., Pinard, P. F., and Dean, A. J., "Experimental and Numerical Investigation of Ejectors for PDE Applications," AIAA Paper 2003-4971, July 2003.

[10] Shehadeh, R., Saretto, S., Lee, S. Y., Pal, S., and Santoro, R. J., "Experimental Study of a Pulse Detonation Engine Driven Ejector," AIAA Paper 2003-4972, July 2003.

[11] John, W. T., Paxson, D. E., and Wernet, M. P., "Conditionally Sampled Pulsejet Driven Ejector Flow Field Using DPIV," AIAA Paper 2002-3231, June 2002.

[12] Gharib, M., Rambod, E., and Shariff, K., "Universal Time Scale for Vortex Ring Formation," *Journal of Fluid Mechanics*, Vol. 360, 1998, pp. 121–140.

[13] Porter, J. L., and Squyers, R. A., "Summary/Overview of Ejector Augmentor Theory and Performance Phase 2: Technical Report," Advanced Technology Center Rept. No. R-91100/9CR-47A, Sept. 1979.

[14] Foa, J. V., *Elements of Flight Propulsion*, Wiley, New York, 1960, p. 103.

[15] White, Frank M., *Fluid Mechanics*, McGraw–Hill, New York, 1979, p. 333.

W. Ng
Associate Editor